A CONSISTENT INTERPOLATION FUNCTION FOR THE SOLUTION OF RADIATIVE TRANSFER ON TRIANGULAR MESHES. II – VALIDATION.

Daniel R. ROUSSE[⌘,§], Fatmir ASLLANAJ[♦], Nizar BEN SALAH[❖], Stéphane LASSUE[✧]

[⌘]T3E Industrial research chair, Dept. Mech. Eng., École de technologie supérieure, Canada

[♦]LEMTA, Nancy-Université, CNRS, France

[❖]LMMP, Ecole Supérieure des Sciences et Techniques De Tunis (ESSTT), 1008 Tunis, Tunisia

[✧]LAMTI, Université d'Artois, France

[§]Correspondence author. Phone: +1 514 396-8800, 7341. Email: Daniel.Rousse@etsmtl.ca

Abstract

This paper presents selected problems used to assess the validity and usefulness of a first-order skew, positive coefficient, upwind scheme (SPCUS) applied to radiative transfer. This particular procedure could be incorporated in several discretization methods such as finite volume, finite element or control volume finite element methods for the prediction of radiative transfer in participating media. The suggested scheme has been validated by application to several basic two-dimensional test problems, acknowledged by the radiative heat transfer community: its performance has proven to be good.

Keywords: radiation, finite volume method, triangular meshes, participating media, validation

Nomenclature

ES	Exponential scheme
US	Upwind scheme
BSUS	Basic Skew Upwind scheme
SPCUS	Skew, positive coefficient, upwind scheme
Q_r	Dimensionless radiative (or radiant) heat flux
P	Node of reference
r	Radiation or Reference point

Greek symbols

γ	σ_s / β
μ	Direction cosine
η	Direction cosine

Subscripts

x	Along axis x
y	Along axis y
r	Radiation

Superscripts

$\rightarrow$	Vectorial quantity
$'$	Incoming direction
m	Discrete direction

Other symbols: *ASME, JHT 1999, 121(4), 770-773.*

1. Introduction

The following acknowledged standard problems were considered to assess the proposed skew positive coefficient upwinding scheme [1]: (1) gray absorbing media in a rectangular enclosure; (2) gray scattering media in a rectangular enclosure; (3) gray absorbing media in a trapezoidal enclosure; (4) gray absorbing, emitting media in a *L*-shaped enclosure; and (5) gray absorbing media in a curved enclosure.

For each demonstration problem, steady-state conditions, homogeneous, constant thermophysical and radiative properties, were considered [2]. No relaxation was used in the computations. The iterations were terminated when the relative value of the residual on the incident radiation *G*, from one iteration to the next, met a prescribed condition $\tilde{\varepsilon}$. In the test problems considered here $\tilde{\varepsilon} = 10^{-6}$ was found to be satisfactory: it yielded solutions that were essentially insensitive to further reductions in $\tilde{\varepsilon}$.

The proposed interpolation scheme was implemented within a Control Volume Finite Element Method (CVFEM) [2]. For ease of implementation, structured-grids, with nodes arranged along straight or curved lines, were employed for all investigations presented here. Nevertheless, although applied to structured meshes herein, the proposed scheme could be implemented on unstructured meshes [3-8] as the ideas are developed about a single finite element [1].

Various ways of forming triangular elements from quadrilaterals were investigated. The angular discretization was always customized so as to match the physical boundaries of the domain with (ϕ,θ) azimuthal-polar discretization, except in regular geometries for which standard (equal weight) S_n discretization were used. Practically, a relatively coarse S_4 angular discretization or a 16 × 4 (ϕ,θ) discretization were found to be sufficient to minimize the error due to the quadrature approximation. For each problem, the refinement was stopped

when further increases in the number of directions does not yield a significant change in the solution.

All relevant details are provided herein to allow the reader to implement the problems in his strategy to validate his own numerical method.

For purely absorbing media the *exact* (reference) solution is calculated with:

$$I_P = I_r e^{-\tau} + I_b(T)(1-e^{-\tau}) \tag{1}$$

where I_r is the intensity at an upstream location along a discrete direction $\vec{\Omega}$, τ is the optical depth between *r* and *P* measured along $\vec{\Omega}$, and $I_b(T)$ is the blackbody intensity at the temperature *T* of the medium.

2. Gray absorbing media in a rectangular enclosure

2.1 Problem statement

In this test case, the proposed CVFEM is applied to a square enclosure (with black walls, $\varepsilon = 1$) filled with an absorbing medium ($\gamma = 0$) at constant temperature T_m = 1. In a first problem, all walls are assumed to be cold (*T* = 0), except for the third wall in Fig. 1, for which $T_3 = 1$. The absorption coefficient is $\kappa = 0.1\text{m}^{-1}$. In a second problem, T_3 is also set to zero. Several optical thicknesses are considered. Here, the dimensionless radiant heat flux, Q_r, is set equal to $q_r / (\tilde{\sigma} T_m^4)$.

2.2 Numerical details and results

The results presented in Fig. 2 show the radiative intensity fields within the domain for the specific S_N direction (μ = 0.797245675, η = 0.577350269). The test case has been

treated by use of a 21×21 regular grid, and with a (equal weight) S_8 quadrature. The profiles provided by the ES, US, BSUS, and SPCUS schemes (detailed in [1]) are compared to the exact solution. As the medium is at the same temperature than wall 3, radiation leaving this wall is maintain at the same level as it travels throughout the domain.

A discontinuity is shown at point (0,0) as there is a physical discontinuity imposed between wall 3 and wall 4. Fig. 2 indicates that along the discontinuity, the ES and US schemes smear the intensity profile: they introduce false scattering (numerical diffusion). This non negligible numerical diffusion is present as these two schemes are considering only one node of influence at the interpolation level. Consequently, the contributions calculated at control volume faces (panels) do not sufficiently take into account the directionality of the propagation of radiation. The BSUS is very good to reproduce the variation of radiative intensity, but spurious numerical oscillations are generated. This is caused by the influence of downstream nodes on the integrated radiant fluxes at control volume faces for specific directions of propagation of radiation. And, as mentioned in the previous section, this produces negative coefficients in the discretization equations. Results for the ISUS are not presented as they are very close to those produced with the SPCUS. Finally, the SPCUS shows is capacity to simulating the discontinuity about point (0,0). It reduces numerical diffusion. This false diffusion is not completely eliminated though: the SPCUS is only first order. However, it is better than standard upwinding to account for directionality.

It should be mentioned at this point that the results presented in Fig. 2 were obtained for a particular orientation of the triangular elements: the longest side of each element was nearly aligned with the selected direction of propagation of radiation for which the discontinuity occurred. When the orientation of the elements changes, results on a coarse grid change. And, as radiation comes from every direction, the grid cannot be aligned with all discrete

directions. In this sense, the ideal scheme should take into account more nodes and present a higher order of approximation. The interested reader should refer to the discussion of Carpentier [9] who compares schemes such as MUSCL with triangular and quadrilateral elements in the context of turbulent fluid mechanics.

In the remainder of the paper, the BSUS will not be considered as the aim is to propose a stable, non oscillating scheme. Moreover, the specifications of commercial CFD codes (such as N3S) exclude such types of schemes.

Results for the second problem are presented in Fig. 3. This figure illustrates the effect of the medium optical thickness, τ, on Q_r, for a square ($L_x/L_y = 1$) black walled (ε = 1) enclosure. Results are presented for three different optical thicknesses, namely, 0.1, 1.0 and 10.0. Other tests were carried out but are not presented. CVFEM solutions were obtained with several schemes but are presented only for the ES, US and SPCUS schemes. Fig. 3 shows that the CVFEM solutions, with a *equal weight* S_4 and 21×21 spatial grid, are in good agreement with the exact reference solution, Equation (1). This result is presented to the reader to indicate that although the US scheme is prone to false scattering, the overall results are acceptable and that the SPCUS scheme produces solutions that are much closer to the reference (exact) solution. The physical interpretation of the results has been discussed elsewhere in [10]. As τ increases, the intensity at any particular point becomes increasingly dependent of its immediate surroundings. For a boundary point, *P*, the incoming intensity is then related to the intensity of a point in the medium very near *P*. As the boundary temperature is zero (zero outgoing radiant heat flux) and the medium temperature is T_m, for τ = 10, Q_r is approximately unity. To capture the discontinuity of temperature at the boundary, mesh enrichment is needed in the vicinity of the walls. Otherwise, the CVFEM cannot accurately predict radiant heat fluxes at the walls showing 20% error for τ = 10.

3. Gray scattering media in a rectangular enclosure

3.1 Problem statement

In the enclosure depicted in Fig. 1, lower surface (wall 4) is maintained at a constant temperature, T_4, and all other surfaces are assumed to be at a constant zero temperature. The medium is assumed to scatter radiation isotropically and does not absorb radiant energy ($\gamma = 1$). Results of the following investigators who studied this problem were considered: Fiveland [11], Truelove [12], Modest [13], Crosbie and Schrenker [14], Their numerical solutions are used as references to check those obtained with the proposed CVFEM with the SPCUS and US schemes. T_4 is used as a reference temperature to obtain suitable non-dimensional quantities. Here, $Q_r = q_r / \tilde{\sigma} T_4^4$, permits a direct comparison with the results presented in the above-listed references. Crosbie and Schrenker [14] proposed an exact solution.

3.2 Numerical details and results

The effects of wall emissivities, aspect ratio, and optical thickness on the dimensionless radiant heat flux, Q_r, at the lower surface, were investigated. For the results presented in this section, a (equal weight) S_4 and 21×21 spatial grid was used. Each rectangular quadrilateral is divided into two triangular elements.

In Fig. 4(a), results are presented for a square enclosure ($L_x / L_y = 1$), with unit optical thickness, $\tau_0 = 1$, having three different surface emissivities, ε, namely 0.1, 0.5, and 1.0

(here each wall of the medium has the same emissivity). Figure 4(a) shows that the CVFEM solutions, for both schemes, are in good agreement with the reference zonal and discrete ordinates solutions, and predictions for a black enclosure ($\varepsilon = 1$) are somewhat more accurate than that obtained by Modest (diamonds) with a differential approximation (DA) [15]. As the emissivity decreases, the intensity leaving a boundary becomes increasingly dependent on the incident intensity on this boundary: as a result, the radiant heat flux at the hot wall becomes increasingly uniform and small with decreasing ε.

The effects of the aspect ratio, L_x/L_y, are presented in Fig. 4(b) for $\tau_0 = 1$ and $\varepsilon = 1$. Again, the results indicate that the CVFEM predictions are in good agreement with those of the zonal method (diamonds) and Crosbie's method [14]. Predictions for high aspect ratios are more precise than those obtained by Modest [15].

The effect of the optical thickness, τ, is shown in Fig. 4(c) for ε = 1 and $L_x/L_y = 1$: the results indicate once more that the proposed CVFEM can successfully predict radiant heat transfer in scattering media having medium (τ = 1) to large (τ = 10) optical thickness, as the predictions are in good agreement with the reference solutions. For τ = 10, the CVFEM and DA results are essentially similar. It is not because CVFEM results deteriorate with increasing optical thickness but simply because the DA is more accurate at high τ. Indeed, the DA or P_1 approximation may be substantially in error in optically thin situations but is very good at high τ [15].

CPU time and convergence rates were also investigated. Comparisons were carried out with respect to the US scheme, for the SPCUS and the ES scheme: The relative CPU time is 1 with the upwind scheme, 1.22 with the SPCUS scheme, and 1.33 for the ES scheme.

For each scheme, it was found that the number of iterations required to obtain a converged solution increases with τ. Convergence is slower with increasing optical thickness because in purely scattering medium with high τ, the reinforcement term in the RTE becomes preponderant as there is strong coupling between directions.

Of course, the CPU time requirement augments linearly with the number of iterations required for convergence:

4. Gray absorbing media in a trapezoidal enclosure

4.1 Problem statement

This test case involves the irregular quadrilateral enclosure depicted in Fig. 5. At the implementation level, the (x – y) coordinates of the four corners in the enclosure were: (0.00, 0.90), (0.36, 1.99), (2.36, 1.99), and (3.03, 0.00). The enclosure is assumed to be filled with an absorbing but non-scattering medium ($\gamma = 0$) at constant temperature T_m, and the walls are assumed to be black and held at a constant zero temperature. A FVM solution for this problem has been proposed [16-18] and is used here as a reference.

4.2 Numerical details and results

Fig. 6 illustrates the effect of the optical thickness of the medium, τ, on the values of the dimensionless radiant heat flux, $Q_r = q_r / 4\tilde{\sigma} T_m^4$, at the top wall. Here, a positive Q_r indicates a flux that leaves the enclosure. A 41×41 spatial grid was required to match the

exact solution faithfully. The angular discretization (16×4) was adjusted to make the projections of the edges of the solid angles match the orientations of the walls.

CVFEM solutions for the radiant heat flux leaving the enclosure via the top wall, obtained with an angular discretization involving 8 directions per octant, are presented for three different optical thicknesses, namely, τ = 0.1, 1.0 and 10.0. Fig. 6 shows that the surface radiant heat fluxes predicted by the proposed CVFEM, with the SPCUS scheme, are in good agreement with the exact solutions. For thick media, the radiation from distant locations is mostly eliminated before it reaches a particular point: the radiative behavior at any point depends only on its immediate surroundings. This provides the incentive to employ a fine spatial mesh in the corners, as there are important changes in the radiant heat flux in these areas, especially for a thick medium. For the limit of a thin medium (τ = 0.1), the surface radiant heat flux depends essentially on surface temperatures. As a result, the radiant heat flux at the top wall decreases with decreasing optical thickness because all surface temperatures are zero.

5. Gray participating media in a *L* -shaped enclosure

5.1 Problem statement

This test case involves the irregular-shaped enclosure shown in Fig. 7. The enclosure is assumed to be filled with an emitting, absorbing, and isotropically scattering medium at constant temperature T_m, and the walls are assumed to be black and held at a constant zero temperature, except for the top wall where $T = T^*$. This is equivalent to assuming an outgoing radiant heat flux, Q_{in}, on the top wall between point A and point E (Fig. 7). Here, the

solutions proposed by Chui [16] using a FVM are used as references. Chai *et al.* [19-21] also used this test case to assess their methods. Q_{in} = 1 and $T_m = 1$ for purposes of comparison with the solutions proposed in Chui [16].

5.2 Numerical details and results

Grid refinement as well as optical thickness effects were investigated. The above-described enclosure involves a particularly interesting feature because the non-orthogonal boundaries make a 45° angle with the *x* – *y* coordinate system shown in Fig. 7. Therefore, it is easy to employ a *boundary matching* angular discretization with at least 2 solid angles per quadrant of the *x* – *y* plane.

Fig. 8 illustrates the dimensionless radiant heat flux, Q_r, at the *left-south* wall, identified by points *A*, *B*, *C*, *I*, and *D* in Fig. 7. In Fig. 8(a) the medium both scatters σ_s = 1.00 and absorbs κ = 0.01 radiant energy while, in Fig. 8(b), the medium absorbs κ = 0.01 radiant energy only. In [16], the investigator employed a relatively coarse 11×4 spatial grid and an angular discretization that involved 2 latitudes and 8 longitudes within an octant. For this test case, the first spatial computational domain employed with the proposed method consisted of 52 irregular quadrilaterals, each divided into two triangular elements, and the angular grid was constructed using 16 discrete directions, that is one latitude in the positive *z* direction and 4 discrete solid angle in each quadrant of the *x* – *y* plane. A finer grid involving 33×15 nodes and 64 directions distributed on two latitudes was also employed for direct comparison with Rousse [10]. In the notation involved in the legend of the figures, the discretization is identified with 4 numbers: the first number refers to the number of grid nodes along the left-south wall (*A*-*B*-*C*-*I*-*D*) and right-north wall (*E*-*F*-*G*-*H*) of the enclosure depicted in Fig. 7; the second number is the number of grid nodes used on the top wall (*A*-*E*) and right wall (*H*-*D*);

the third number refers to the number of latitudes employed with the azimuthal angular discretization; and the last number is the number of solid-angle projections in each quadrant of the $x - y$ plane.

In Fig. 8(a), the surface radiant heat flux, Q_r, along the left-south wall (*A-B-C-I-D*), decreases with the distance away from point *A*, measured between *A* and *D*, because radiation is attenuated by absorption and scattering as it travels away from the top (hot) wall. When there is no scattering ($\gamma = 0$) in Fig. 8(b), the radiant heat flux impinging on a surface is very sensitive to the orientation of this surface with respect to the source Q_{in} (located on the top wall).

In Fig. 8(b) it can be observed that the FVM (11×4) fails to predict the two bumps, that correspond to locations *B* and *C*, in the surface radiant heat flux distribution. Chui's solution [16] indicates a plateau while the (13×4) CVFEM solution shows the two peaks at point *B* and *C*. The CVFEM solution for a coarse grid is shown somewhat better than its corresponding FVM counterpart. This may be caused by the treatment of the boundary conditions and by the fact that in the CVFEM each quadrilateral is divided into two triangular elements. This yields a finer discretization and hence a better approximation of the radiative fluxes across control volume surfaces.

The orientation of the wall changes at *B* and *C*, and this makes the left-south wall lie in a more direct line of sight from the source of radiation on the top wall (*A-E*). There should be discontinuities in the Q_r distribution at *B* and *C* for $\sigma_s = 0$. The tendency is well predicted by the relatively fine grid (33×15 nodes) combined with fine angular discretization involving 64 directions (2 latitudes and 8 projections per quadrant). To capture the flux discontinuities,

grid points should be inserted close to points *B* and *C*. Beyond point *C*, along *C*-*D*, after the step *B*-*C*, the radiant heat flux is seen to decrease to zero as some points (beyond point *I*) do not "see" the radiation source on the top wall *A*-*E*, and because there is no reflection and no emission from the boundaries. When scattering is present, Fig. 8(a), the changes in the distribution of the radiant heat flux at point *B* and *C* are less pronounced because a direct line of sight to *A*-*E* is less important than in the case of no scattering in Fig. 8(b). Chui's solution [16] and the coarse CVFEM solution indicate monotonic decrease of the radiant heat flux along the left-south wall, whereas the CVFEM solution obtained with a fine grid, which reproduces the physics more faithfully, shows the expected bumps at point *B* and *C*.

The radiant heat flux at the *right-north* wall (*E*-*F*-*G*-*H* in Fig. 7) was also computed [10] (but not shown here in) with more accuracy with the CVFEM than with the FVM of Chui [16]. The effect of angular and spatial discretization refinement and that of optical thickness were also investigated. Interested readers should consult the corresponding author for details.

6. Gray absorbing media in a curved enclosure

6.1 Problem statement

In this last test case for pure radiative heat transfer, a quarter of circle – with a rectangular region added on its top – was used as a test geometry (Fig. 9). The curve wall is hot, $T_4 \neq 0$, and black while all other walls are cold, $T_1 = T_2 = T_3 = 0$. The medium is cold and purely absorbing with $\kappa = 1$. The radius of the quarter of circle is equal to the length along the *x*-axis, $L_x = 1.0$, and $L_y = 1.5$. Chai *et al.* [20, 21] and Liu *et al.* [22] also studied that problem.

6.2 Numerical details and results

A 37×37 spatial grid and an angular discretization 20×4 in the ϕ and θ directions were employed with a progressive deployment of the spatial grid: there are more nodes in the immediate vicinity of the walls.

The predictions of the radiant heat flux on the right wall (wall 2) are reported in Fig. 10. It is shown that the CVFEM solution, using the US scheme, is in good agreement with that proposed by Chai *et al.* [21].

As the hot wall is curved, it is impossible on this surface to customize the angular discretization in order to have solid angle edges match the boundaries exactly for each boundary element. If the value of the incoming flux at this surface was the quantity of interest or if the curved wall was reflecting, a special treatment for the boundary conditions would be required. However, as this curved surface is black (no reflection), such a treatment is not necessary here: only the outgoing flux is needed on the curved boundary.

7. Conclusion

This paper presented the detailed two-dimensional validation procedure of a skew, positive coefficients, upwind scheme (SPCUS) for the computation of radiative transfer in enclosures filled with participating media.

The proposed scheme is based on the application of sound physical arguments, resulting in: (1) fast convergence of the algorithm; (2) inherent preclusion of the possibility of computing

negative coefficients to the discretized algebraic equations; (3) relatively low levels of false scattering; (4) relative insensitivity to grid orientation; and (5) solutions completely free from undesirable oscillations. These attributes render the scheme attractive, especially in the context of combined modes of heat transfer and fluid flow for which CPU time is a major concern.

However, results show that despite the superiority of the SPCUS scheme over the upwind scheme or exponential scheme, in adequately predicting the discrete value of the radiative intensity in one particular direction, when integrated values are calculated (heat fluxes, for instance), the errors are more or less averaged over all directions. Hence, despite an increase of about 20% in computational time requirement, the difference between the SPCUS scheme and the simple US diminishes substantially.

Acknowledgements – The authors acknowledge Rodolphe Vaillon (CNRS researcher, CETHIL, INSA de Lyon) and Guillaume Gautier (CSN) for their collaboration during these research works. The authors are also grateful to the Natural Sciences and Engineering Research Council of Canada (NSERC). Thanks go to Alan Wright for helping in the preparation of this manuscript.

References

[1] D. R. Rousse, F. Asllanaj, A consistent interpolation function for the solution of radiative transfer on triangular meshes. I – Comprehensive formulation, Num. Heat Transfer B, (submitted), 2010.

[2] D. R. Rousse, Numerical Predictions of Two-Dimensional Conduction, Convection, and Radiation Heat Transfer. I – Formulation, Int. J. Thermal Sciences, vol. 39 (3), pp. 315-331, 2000.

[3] M. Sakami, and A. Charette. Application of a modified discrete ordinates method to two-dimensional enclosures of irregular geometry. J. Quant. Spectrosc. Radiat. Transfer, vol. 64 (3), pp. 275–298, 2000.

[4] M. Y. Kim, S. W. Baek, and J. H. Park, Unstructured finite-volume method for radiative heat transfer in a complex two-dimensional geometry with obstacles, Num. Heat Transfer B, vol. 39 (6), pp. 617-635, 2001.

[5] M. Y. Kim, S. W. Baek, and S. I. Park, Evaluation of the finite-volume solutions of radiative heat transfer in a complex two-dimensional enclosure with unstructured polygonal meshes, Num. Heat Transfer B, vol. 54 (2), pp. 116-137, 2008.

[6] C. Kim, M. Y. Kim, M. J. Yu, and S. C. Mishra, Unstructured polygonal finite volume solutions of radiative heat transfer in a complex axisymmetric enclosure, Num. Heat Transfer B, vol. 57 (3), pp. 227-239, 2010.

[7] M. Ben Salah, F. Askri, and S. Ben Nasrallah, Unstructured control-volume finite-element method for radiative heat transfer in a complex 2-D geometry, Num. Heat Transfer B, vol. 48 (5), pp. 477-497, 2005.

[8] F. Asllanaj, V. Feldheim, and P. Lybaert. Solution of radiative heat transfer in 2-D geometries by a modified finite volume method based on a cell vertex scheme using unstructured triangular meshes, Num. Heat Transfer B, vol. 51 (2), p. 97-119, 2007.

[9] R. Carpentier, Comparaison entre des Schémas 2D de Type Roe sur Maillage Régulier Triangle ou Quadrangle. I: Calcul au Sommet – Pentes Centrées, Technical Report, INRIA, no. 2824, 1996.

[10] D. R. Rousse, G. Gautier, and J. F. Sacadura, Numerical Predictions of Two-Dimensional Conduction, Convection, and Radiation Heat Transfer. II – Validation, Int. J. Thermal Sciences, vol. 39 (3), pp. 332-353, 2000.

[11] W. A. Fiveland, Discrete-Ordinates Solutions of the Radiative Transport Equation for Rectangular Enclosures, ASME J. Heat Transfer, vol. 106 (2), pp. 699-706, 1984.

[12] J. S. Truelove, Discrete-Ordinates Solutions of the Radiation Transport Equation, ASME J. Heat Transfer, vol. 109 (4), pp. 1048-1052, 1987.

[13] M. F. Modest, Radiative Equilibrium in a Rectangular Enclosure Bounded by Gray Walls, J. Quant. Spectros. Radiat. Transfer, vol. 15, pp. 445-461, 1975.

[14] A. L. Crosbie, and P. Schrenker, Radiative Transfer in a Two-Dimensional Rectangular Medium Exposed to Diffuse Radiation, J. Quant. Spectros. Radiat. Transfer, vol. 31, pp. 339-372, 1984.

[15] M. F. Modest, Radiative Heat Transfer, 2nd Ed., Academic Press, New York, 2003.

[16] E. H. Chui, Modelling of Radiative Heat Transfer in Participating Media by the Finite Volume Method, Ph.D. thesis, University of Waterloo, Canada, 1990.

[17] G. D. Raithby, and E. H. Chui, A Finite-Volume Method for Predicting Radiant Heat Transfer in Enclosures with Participating Media, ASME J. Heat Transfer, vol. 112 (2), pp. 415-423, 1990.

[18] E. H. Chui, and G. D. Raithby, Computation of Radiant Heat Transfer on a Non-Orthogonal Mesh using the Finite Volume Method, Num. Heat Transfer B, vol. 23, pp. 269-288, 1993.

[19] J. C. Chai, H. S. Lee, and S. V. Patankar, Improved Treatment of Scattering using the Discrete Ordinates Method, ASME J. Heat Transfer, vol. 116, pp. 260-263, 1994.

[20] J. C. Chai, H. S. Lee, and S. V. Patankar Treatment of Irregular Geometries using a Cartesian Coordinates Finite-Volume Radiation Heat Transfer Procedure, Num. Heat Transfer B, vol. 26, pp. 225-235, 1994.

[21] J. C. Chai, G. Parthasarathy, H. S. Lee, and S. V. Patankar, Finite-Volume Radiative Heat Transfer Procedure for Irregular Geometries, J. Thermophys. Heat Transfer, vol. 9, pp. 410-415, 1997.

[22] J. Liu, M. Shang, and Y. S. Chen, Prediction of Radiative Transfer in General Body-Fitted Coordinates, Num. Heat Transfer B, vol. 31, pp. 423-439, 1997.

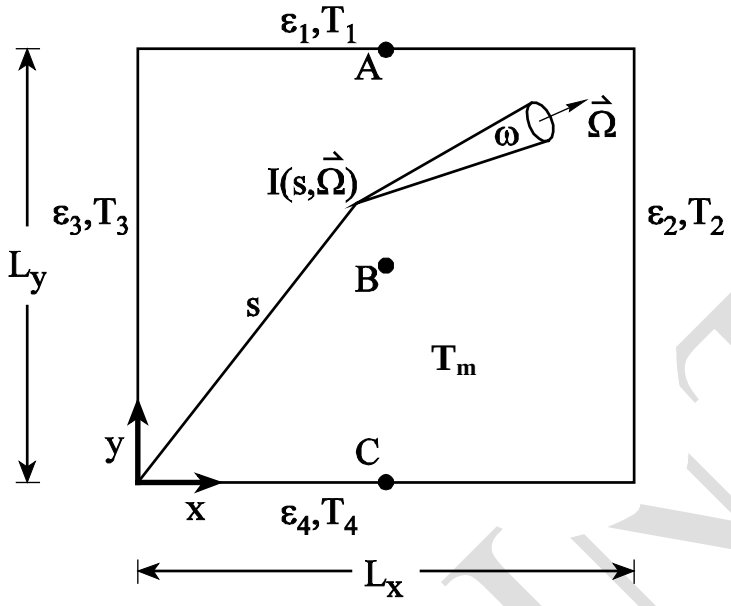

Figure 1: Rectangular enclosure: problem schematic

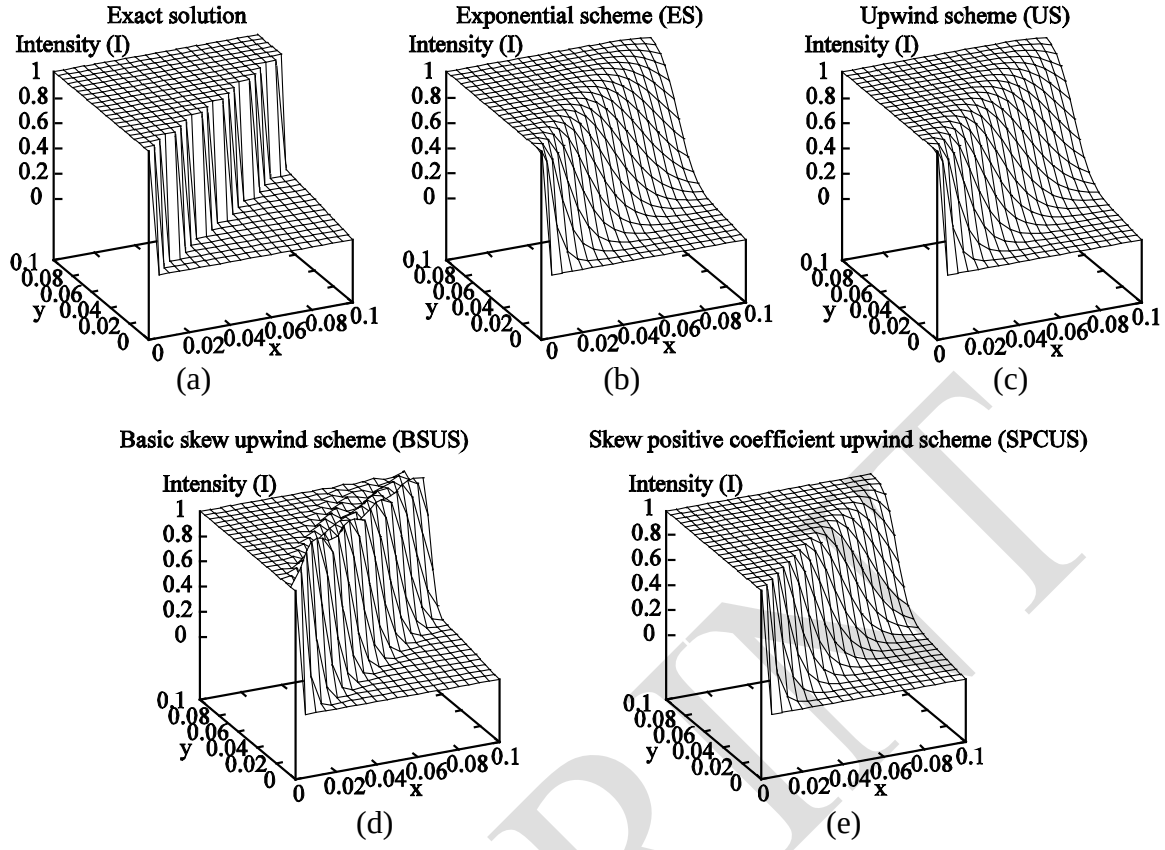

Figure 2: Spatial distribution of radiative intensity for discrete direction (μ = 0.797245675, η = 0.577350269) in a purely absorbing medium (T_3 = 1.0, and κ = 0.1 m^{-1}): (a) exact solution; (b) Exponential scheme; (c) Upwind scheme; (d) Basic skew upwind scheme; (e) Skew positive coefficient upwind scheme.

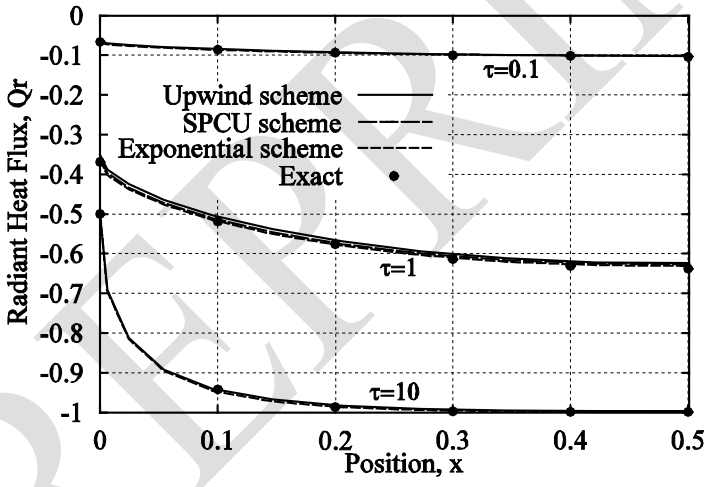

Figure 3: Distribution of dimensionless surface radiant heat flux, Q_r, for non-scattering absorbing media, γ = 0. Effect of optical thickness, τ, with ε = 1, and X/Y = 1.

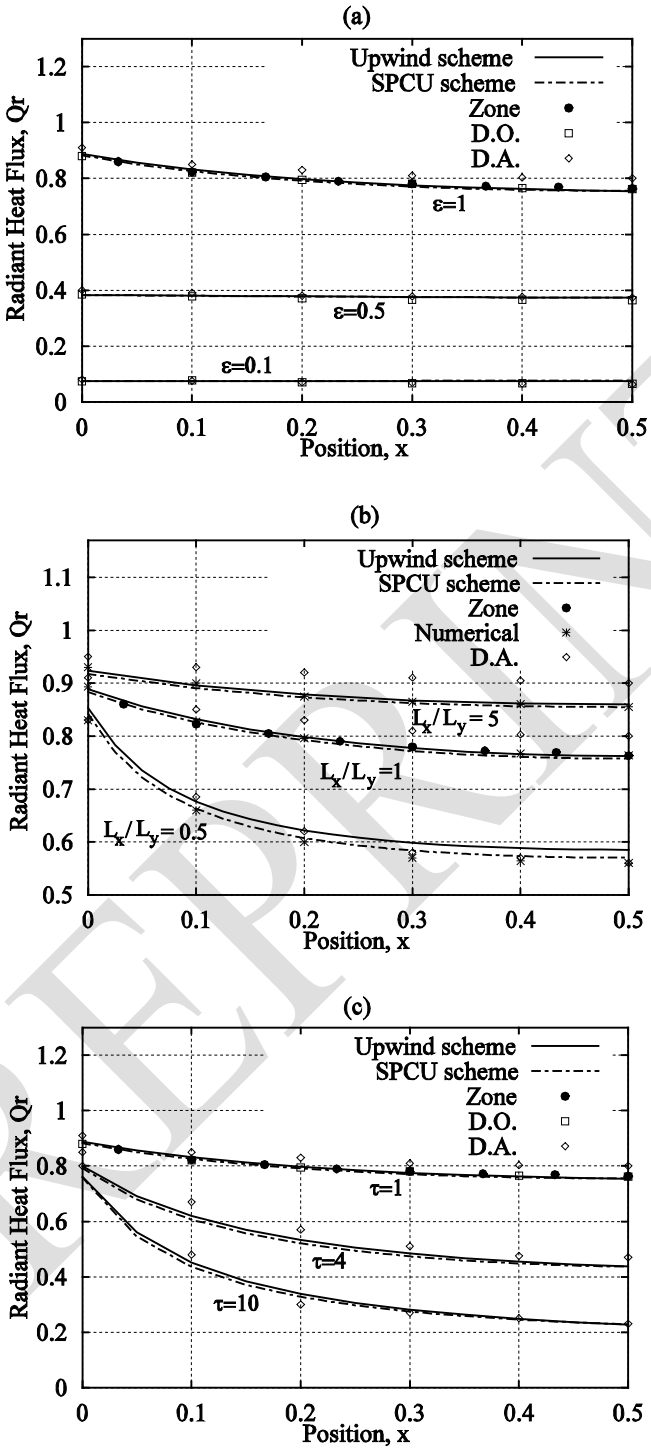

Figure 4: Distribution of dimensionless bottom surface radiant heat flux, Q_r, for scattering, non-absorbing media (γ = 1): (a) Effect of wall emissivity, ε, with L_x/L_y = 1 and τ_0 = 1; (b) Effect of aspect ratio, L_x/L_y, with ε = 1 and τ_0 = 1; and (c) Effect of optical thickness, τ_0, with L_x/L_y = 1 and ε = 1.

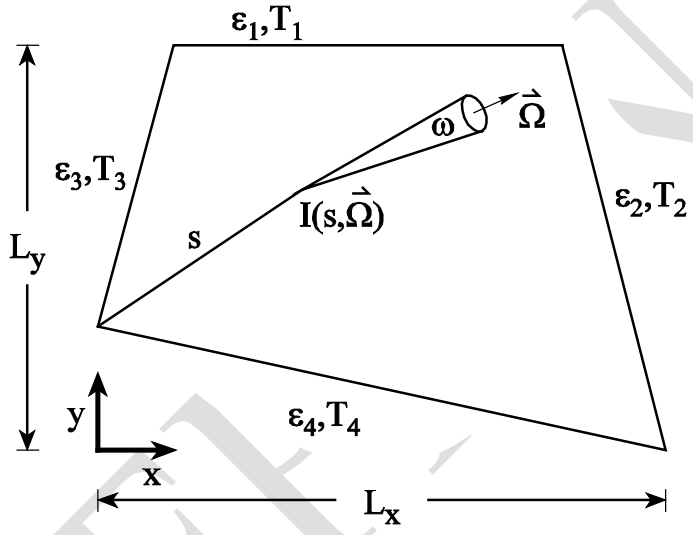

Figure 5: Trapezoidal enclosure: problem schematic.

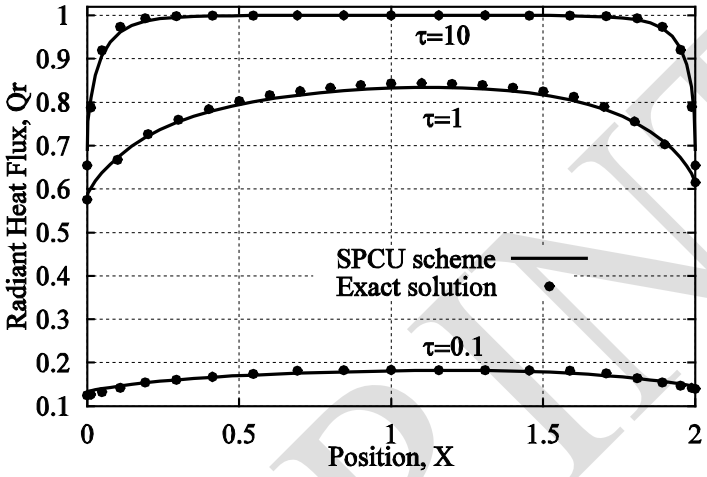

Figure 6: Dimensionless radiant heat flux on the top surface for absorbing media bounded by a black trapezoidal enclosure: Effect of optical thickness, τ .

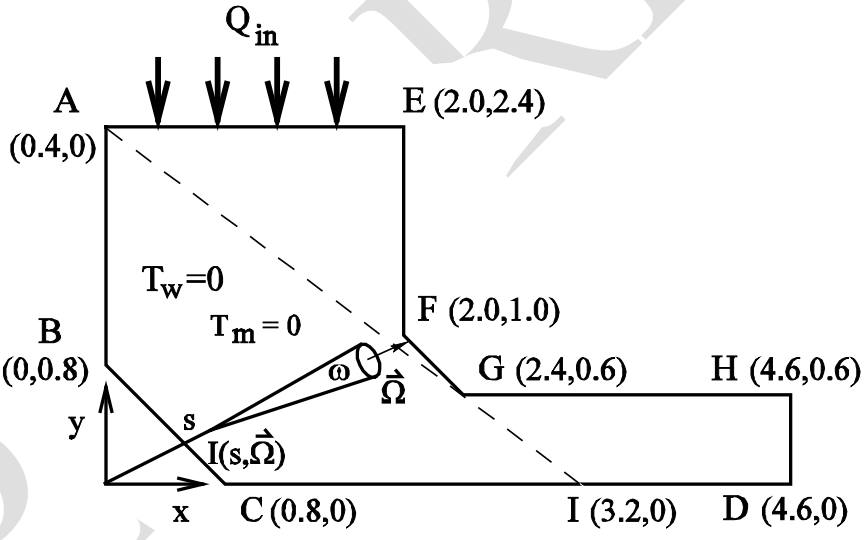

Figure 7: *L*-shaped two-dimensional enclosure: problem schematic.

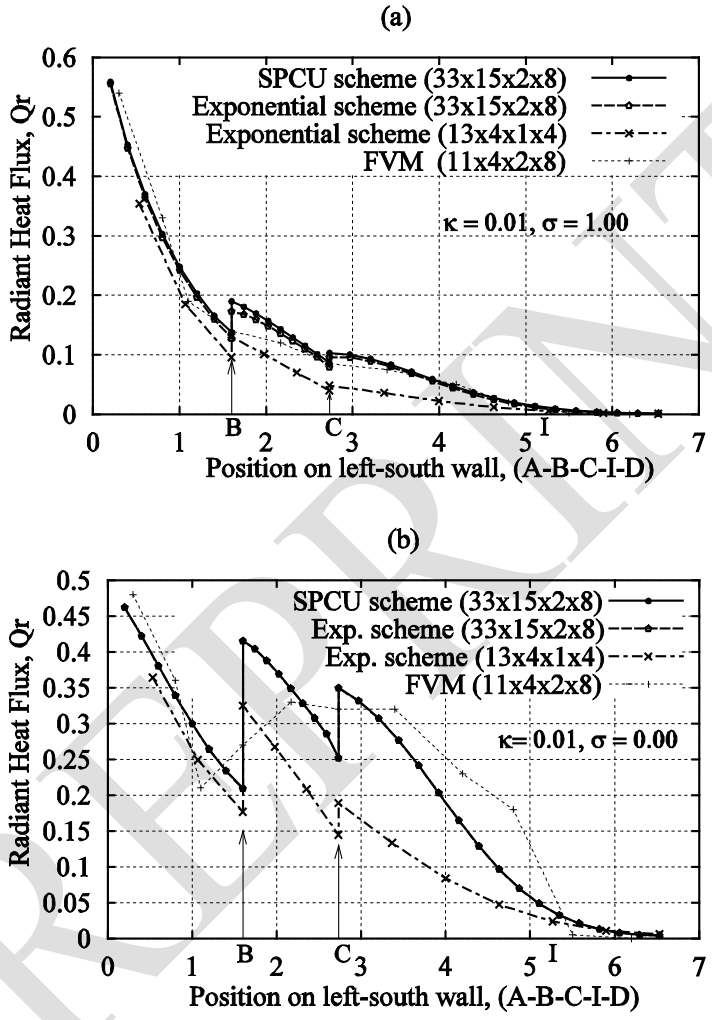

Figure 8: Distribution of dimensionless radiant heat flux, Q_r, on the left-south wall *A-B-C-I-D* for : (a) κ = 0.01, σ_s = 1.0; (b) κ = 0.01, σ_s = 0.0.

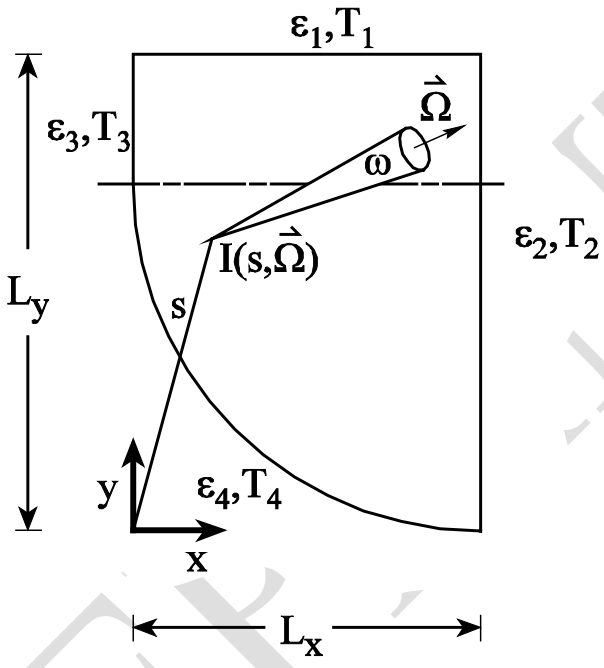

Figure 9: Curved computational enclosure: problem schematic.

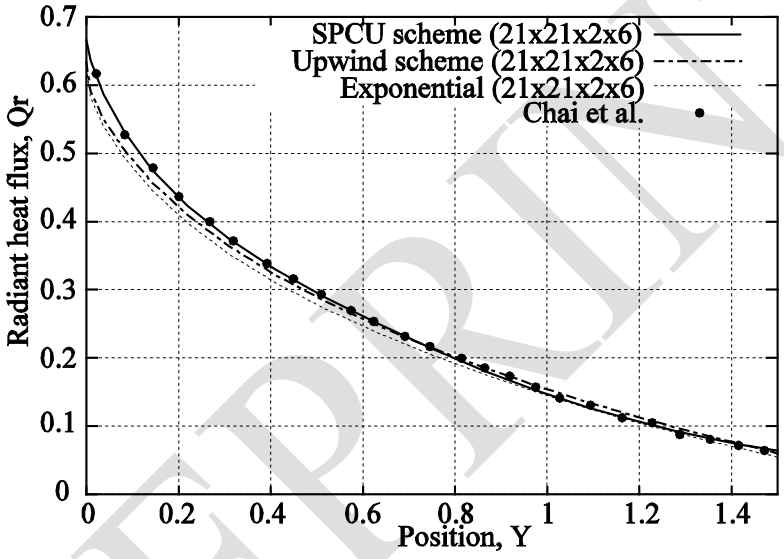

Figure 10: Distribution of dimensionless radiant heat flux, Q_r, on the right surface for absorbing media bounded by a black curved enclosure, β = 1.